In-Plane Deformation Analysis and Design of Experiments Approach for Injection Molding of Light Guide Plate for LCDs

Ho-Sang Lee[1,#]

1 Department of Mechanical Design Engineering, Chungju National University, Chungju, Chungbuk, South Korea
Corresponding Author / E-mail: lhs@chungju.ac.kr, TEL: +82-43-841-5375, FAX: +82-43-841-5370

KEYWORDS : Injection Molding, Finite Element Analysis, Light Guide Plate, Design of Experiments, Brightness

A computer code was developed to simulate both the thermal stresses introduced during the post-filling stage and the in-plane deformation after ejection process by finite element method based on the plane stress theory. The computer simulation was applied to the mold design of a 2 inch light guide plate (LGP) for thin film transistor (TFT)-liquid crystal displays (LCD). With injection molding experiments based on the design of experiments (DOE) technique, the influences of the processing conditions in injection molding on brightness and uniformity of the LGP were investigated, and the optimal processing parameters were selected to increase the brightness and uniformity. The verification experiment showed that the brightness and uniformity of the LGP were increased dramatically under the selected optimal processing conditions.

Manuscript received: August 27, 2004 / Accepted: June 30, 2005

1. Introduction

In the area of computer and communication, the liquid crystal display (LCD) has emerged as the most successful display technology because it meets the critical requirement for portability, low power, and full color generation. The liquid crystal inside the glass panel is arranged in a certain direction and angle by the electric signal delivered from the integrated circuit (IC) driver. A cold cathode fluorescent lamp (CCFL) is mounted along the top and bottom edges of the panel to illuminate the background of the display panel. The CCFL reflector prevents the light from leaking in every direction and reflects the light that transmits out of the opposite side back to the light guide plate (LGP) and maximizes the efficiency of the lamp. In the backlight unit, the light rays from the source are incident on one of the sides of the LGP and are guided inside the LGP based on the principle of total internal reflection. For the display to be viewed comfortably under a variety of ambient light conditions ranging from dark to full sunlight, the LGP should provide adequate brightness and uniformity of brightness, while minimizing the power consumption.

The LGP is a thin injection molded plastic part, which exhibits residual stresses and deformation after molding. The deformation of the plastic product is primarily due to the non-uniform differential shrinkages within the part, which lead to the development of uneven residual stresses. In essence, both the thermal expansion and the stiffness of the material, coupled with the transient temperature gradient within the material, contribute to the formation of the thermal stresses. The demands for high dimensional stability and close dimensional tolerances require knowledge of the deformation mechanisms of the plastic LGP with thermal stresses.

Several attempts have been made to theoretically predict residual stresses and deformation in injection molded parts. With a simple elastic material behavior model, Jacques [1] estimated the stresses and the effects of unbalanced cooling on the warpage of flat, amorphous, injection molded parts, employing a one-dimensional finite difference analysis of the temperature profile through the part thickness. Tamma and Railkar [2,3] presented finite element and transfinite element formulations to obtain the solution for the combined thermal and stress analysis of injection molded parts. The stress distributions and warpage were predicted in a cantilever beam-type part. Razayat and Stafford [4] modified the one-dimensional thermal residual stress theory of Lee et al. [5] with a transversely isotropic linear viscoelastic model for predicting the thermally induced residual stress of the injection molded part. Chang and Tsaur [6,7] developed an integrated theory and computer program for simulation of shrinkage, warpage, and sink marks of crystalline polymer injection molded parts. The basic theory considered filling, packing, cooling, the polymer viscoelastic behavior, the PvT and crystalline behavior of the polymer. Also, they carried out the structural analysis after ejection of the part from the mold. Liu [8] proposed a viscoelastic phase transformation model, using a standard linear solid model to represent the solidified polymer and a viscous fluid model to represent the polymer melt. Also a 2-D finite element scheme was applied to predict the residual stress and warpage within the injection molded parts induced during the cooling stage of the injection molding cycle. Santhanam [9] adopted an analogous model to study the residual stress development and post-molding deformation in a strip cavity. The analysis was also extended to thin three-dimensional molded parts, making use of a local treatment. Most of the previous studies were confined to proposing models that could be applied to residual stress analysis. Furthermore the deformation of the part has been focused in the study of plate bending behavior.

In this paper, the previous study [10] was modified to consider the variations of thermal conductivity and specific heat as a function of temperature. The developed finite element program based on the plane stress theory predicts both the thermal stresses introduced during the post-filling and the in-plane deformation after ejection of the part from the mold. The simulation was applied to a 2 inch sized LGP for the TFT-LCD to design the mold cavity. With injection molding experiments based on DOE technique, the influences of the processing conditions in injection molding on brightness and uniformity of the LGP were investigated, and the optimal processing parameters were selected to increase the brightness and the uniformity of the LGP.

2. Finite Element Analysis

2.1 Flow Analysis

For an arbitrary planar geometry, an approach similar to that of Chiang et al. [11] was used for the flow analysis. The Hele-Shaw approximation can be applied in the momentum equation of the flow analysis because the thickness of injection molded parts is usually very small compared with other dimensions. In addition, heat conduction in the plane was assumed to be negligible compared with the conduction in the thickness direction. The relevant governing equations for the continuity, momentum, and energy are described as:

$$\frac{\partial \rho}{\partial t}+\frac{\partial}{\partial x}(\rho v_x)+\frac{\partial}{\partial y}(\rho v_y)=0 \tag{1}$$

$$\frac{\partial}{\partial z}(\eta\frac{\partial v_x}{\partial z})-\frac{\partial P}{\partial x}=0 \tag{2}$$

$$\frac{\partial}{\partial z}(\eta\frac{\partial v_y}{\partial z})-\frac{\partial P}{\partial y}=0 \tag{3}$$

$$\rho C_p(T)(\frac{\partial T}{\partial t}+v_x\frac{\partial T}{\partial x}+v_y\frac{\partial T}{\partial y})=\frac{\partial}{\partial z}(\kappa(T)\frac{\partial T}{\partial z})+\eta\dot{\gamma}^2 \tag{4}$$

where ρ is the density; t, the time; P, the pressure; η, the viscosity; T, the temperature; C_p, the specific heat; κ, the thermal conductivity; $\dot{\gamma}$, the shear rate; x and y, the planar directions; z, the gapwise direction; and v_x and v_y, the velocity components in x and y directions, respectively.

Considering the no-slip and symmetric boundary conditions on velocity, equations of continuity and momentum can be integrated as:

$$\frac{\partial}{\partial x}(S\frac{\partial P}{\partial x})+\frac{\partial}{\partial y}(S\frac{\partial P}{\partial y})=G\frac{\partial P}{\partial t}+F \tag{5}$$

with:

$$S=\int_0^b\rho\int_z^b\frac{z}{\eta}dzd\bar{z} \tag{6}$$

$$G=\int_0^\delta(\frac{\partial\rho_l}{\partial P})_T dz+\int_\delta^b(\frac{\partial\rho_s}{\partial P})_T dz \tag{7}$$

$$F=\int_0^\delta(\frac{\partial\rho_l}{\partial T})_P\frac{\partial T}{\partial t}dz+\int_\delta^b(\frac{\partial\rho_s}{\partial T})_P\frac{\partial T}{\partial t}dz+(\rho_l-\rho_s)_{z=\delta}\frac{\partial\delta}{\partial t} \tag{8}$$

where b is the half thickness, δ is the coordinate of the solid-melt interface, and the subscript l and s denote the liquid and solid states, respectively.

The shear thinning behavior of the viscosity is characterized by the modified-Cross model as follows:

$$\eta(\dot{\gamma},T,P)=\frac{\eta_o(T,P)}{1+(\frac{\eta_o\dot{\gamma}}{\tau^*})^{(1-n)}} \tag{9}$$

For amorphous thermoplastics, η_o can be represented by WLF form as:

$$\eta_o=\begin{cases}D_1\exp\left[\dfrac{A_1(T-T^*)}{A_2+(T-T^*)}\right] & T>T^*\\ \infty & T\le T^*\end{cases} \tag{10}$$

with:

$$T^*=D_2+D_3P \tag{11}$$

$$A_2=\tilde{A}_2+D_3P \tag{12}$$

where $n,\tau^*,A_1,\tilde{A}_2,D_1,D_2$ and D_3 are material constants.

For considering the compressibility effect, two-domain Tait equation of state can be described by

$$v(P,T)=\begin{cases}(a_{os}+a_{1s}(T-T_g))(1-0.0894\ln(1+\dfrac{P}{B_s})) & T\le T_g\\ (a_{om}+a_{1m}(T-T_g))(1-0.0894\ln(1+\dfrac{P}{B_m})) & T>T_g\end{cases} \tag{13}$$

with:

$$T_g=T_{go}+B_2P \tag{14}$$

$$B_m=B_{om}e^{-B_{1m}T} \tag{15}$$

$$B_s=B_{os}e^{-B_{1s}T} \tag{16}$$

where v is the specific volume, and $a_{os},a_{om},a_{1s},a_{1m},B_{0s},B_{0m},B_{1s},B_{1m},B_2$ and T_{go} are material parameters for the specific volume.

The specific heat can be described as a function of temperature for amorphous polymers:

$$C_p(T)=C_1+C_2\bar{T}+C_3\tanh(C_4\bar{T}) \tag{17}$$

with:

$$\bar{T}=T-C_5 \tag{18}$$

where C_1,C_2,C_3,C_4 and C_5 are parameters of the material.

The thermal conductivity is also described as follows:

$$\kappa(T)=\lambda_1+\lambda_2\hat{T}+\lambda_3\tanh(\lambda_4\hat{T}) \tag{19}$$

with:

$$\hat{T}=T-\lambda_5 \tag{20}$$

where $\lambda_1,\lambda_2,\lambda_3,\lambda_4$ and λ_5 are parameters of the material.

The finite element/finite difference methods[12] are employed to solve the coupled equations of Eq. (4) and Eq. (5). The pressure and temperature distributions obtained from the flow analysis are used in the thermal stresses and deformation analysis.

2.2 In-Plane Deformation Analysis

In-plane deformation is caused by the non-uniform shrinkage, which is a consequence of non-uniform pressure and temperature distribution within the cavity. The thermal stresses caused by the non-uniform shrinkage can be effectively calculated by using the thermal expansion coefficient, which is a function of pressure and temperature obtained from the Tait equation. It is assumed that no residual stress is developed until the temperature reaches the glass transition temperature and the parts in solid state are elastic.

Based on plane stress states, the governing equations can be described by the following equations:

Equations of Equilibrium:

$$\frac{\partial\sigma_{xx}}{\partial x}+\frac{\partial\sigma_{xy}}{\partial y}=0 \tag{21}$$

$$\frac{\partial\sigma_{xy}}{\partial x}+\frac{\partial\sigma_{yy}}{\partial y}=0 \tag{22}$$

Strain-Displacement Relations:

$$\varepsilon_{xx}=\frac{\partial\delta_x}{\partial x},\ \varepsilon_{yy}=\frac{\partial\delta_y}{\partial y},\ 2\varepsilon_{xy}=\frac{\partial\delta_x}{\partial y}+\frac{\partial\delta_y}{\partial x} \tag{23}$$

Stress-Strain Relations:

$$\sigma = C(\varepsilon - \varepsilon_o) + \sigma_o = C\varepsilon + f \tag{24}$$

with:

$$\sigma = \{\sigma_{xx} \quad \sigma_{yy} \quad \sigma_{xy}\}^T \tag{25}$$

$$\varepsilon_o = \{\alpha\Delta T \quad \alpha\Delta T \quad 0\}^T \tag{26}$$

$$C = \begin{bmatrix} C_{11} & C_{12} & 0 \\ C_{12} & C_{22} & 0 \\ 0 & 0 & C_{33} \end{bmatrix} \tag{27}$$

$$f = \{f_{xx} \quad f_{yy} \quad f_{xy}\}^T = -C\varepsilon_o + \sigma_o \tag{28}$$

where σ_o is the initial residual stress; α, the linear thermal expansion coefficient; C_{ij} (= C_{ji}), the elastic constants for an orthotropic material; and δ_x and δ_y are the displacements in x and y directions, respectively. C_{ij} are expressed in terms of the engineering constants given below:

$$C_{11} = \frac{E_1}{1-\nu_{12}\nu_{21}}, \quad C_{22} = \frac{E_2}{1-\nu_{12}\nu_{21}}$$

$$C_{12} = \nu_{21}C_{11} = \nu_{12}C_{22}, \quad C_{33} = G_{12} \tag{29}$$

The linear thermal expansion coefficient, α, can be expressed as a function of pressure and temperature by using the Tait equation (Eq. (13)):

$$\alpha = \frac{1}{3v}\left(\frac{\partial v}{\partial T}\right) \tag{30}$$

In order to obtain the finite element formulation for a plane stress problem, δ_x and δ_y are approximated with the shape function ψ_j as follows:

$$\delta_x(x,y) = \sum_{j=1}^{M} \delta_{xj}\psi_j(x,y)$$
$$\delta_y(x,y) = \sum_{j=1}^{M} \delta_{yj}\psi_j(x,y) \tag{31}$$

Using Eq. (31), the Galerkin weighted-residual equations corresponding to the governing equations can be derived as follows:

$$\begin{bmatrix} K_{ij}^{11} & K_{ij}^{12} \\ K_{ij}^{21} & K_{ij}^{22} \end{bmatrix} \begin{Bmatrix} \delta_x \\ \delta_y \end{Bmatrix} = \begin{Bmatrix} F_i^1 \\ F_i^2 \end{Bmatrix} \tag{32}$$

with:

$$K_{ij}^{11} = \int_\Omega h\left(C_{11}\frac{\partial\psi_i}{\partial x}\frac{\partial\psi_j}{\partial x} + C_{33}\frac{\partial\psi_i}{\partial y}\frac{\partial\psi_j}{\partial y}\right)d\Omega$$

$$K_{ij}^{12} = \int_\Omega h\left(C_{12}\frac{\partial\psi_i}{\partial x}\frac{\partial\psi_j}{\partial y} + C_{33}\frac{\partial\psi_i}{\partial y}\frac{\partial\psi_j}{\partial x}\right)d\Omega$$

$$K_{ij}^{22} = \int_\Omega h\left(C_{33}\frac{\partial\psi_i}{\partial x}\frac{\partial\psi_j}{\partial x} + C_{22}\frac{\partial\psi_i}{\partial y}\frac{\partial\psi_j}{\partial y}\right)d\Omega$$

$$K_{ij}^{21} = K_{ji}^{12}$$

$$F_i^1 = \int_\Gamma h\psi_i t_x d\Gamma - \int_\Omega h\left(\frac{\partial\psi_i}{\partial x}f_{xx} + \frac{\partial\psi_i}{\partial y}f_{xy}\right)d\Omega$$

$$F_i^2 = \int_\Gamma h\psi_i t_y d\Gamma - \int_\Omega h\left(\frac{\partial\psi_i}{\partial x}f_{xy} + \frac{\partial\psi_i}{\partial y}f_{yy}\right)d\Omega \tag{33}$$

where h is the part thickness, and f_{xx}, f_{xy} and f_{yy} can be approximated by using the shape functions as:

$$f_{xx}(x,y) = \sum_{j=1}^{M}(f_{xx})_j\psi_j(x,y)$$
$$f_{xy}(x,y) = \sum_{j=1}^{M}(f_{xy})_j\psi_j(x,y) \tag{34}$$
$$f_{yy}(x,y) = \sum_{j=1}^{M}(f_{yy})_j\psi_j(x,y)$$

The boundary tractions, t_x and t_y are as follows:

$$t_x = \sigma_{xx}n_x + \sigma_{xy}n_y$$
$$t_y = \sigma_{xy}n_x + \sigma_{yy}n_y \tag{35}$$

We can reasonably assume that the deformation of a polymer part in a mold cavity is prevented by the mold wall, so the residual stresses of the part before ejection can be obtained from Eq. (23), Eq. (24), and Eq. (32) by using the zero displacement boundary conditions along the cavity boundary. The ΔT, indicated in Eq. (26), is the difference between the gapwise averaged temperature and the glass transition temperature at each node. After the polymer part is ejected from the mold, its residual stresses are redistributed, and this redistribution causes the post-molding deformation of the part. For the post-molding deformation analysis, the molded parts are treated as unconstrained structures, because the loading induced by the injection molding process is self-balanced. To prevent free rigid body motions, a system of statically determinate constraints is applied, avoiding self-straining of the molded part. The boundary conditions after ejection were described in detail in a previous study [10].

The concept of computer code developed for in-plane deformation analysis is shown in Fig. 1

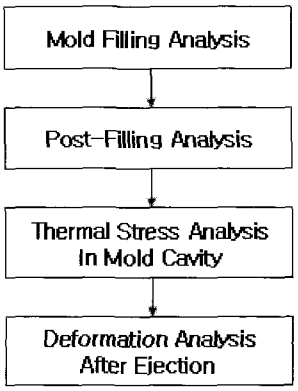

Fig. 1 Flow chart of the deformation analysis

3. Simulated Results

The developed simulation program was applied to the mold design of a 2 inch sized LGP for TFT-LCD. Polycarbonate (Teijin Chem/PC Panlite L-1225L) was used for the LGP. The material data are listed in Tables 1 and 2 [13]. The material parameters for the specific heat, $C_p(J/Kg^oC)$, in Eq. (17) and thermal conductivity, $\kappa(W/m^oC)$, in Eq. (19) are as follows:

$$(C_1, C_2, C_3, C_4, C_5) = (1706.59,\ 2.524,\ 131.726,\ 0.06,\ 417.15)$$

$$(\lambda_1, \lambda_2, \lambda_3, \lambda_4, \lambda_5) = (0.2388,\ 7.15\times10^{-4},\ -0.021,\ 0.03,\ 417.15)$$

The values of elastic modulus and Poisson's ratio used for stress and deformation analysis are $E = 2{,}800MP_a$ and $\nu = 0.38$, respectively.

Fig.2 shows a LGP cavity with a fan gate, whose dimensions are L1=L2=47.389 mm and H1=H2=35.105 mm. To maintain the reflected light uniformly over the upper surface of the LGP, the thickness was designed to be variable like that of a convex lens. Processing conditions used are given in Table 3. Several simulations were carried out to find the optimal gate location satisfying simultaneous filling in both sides of the mold cavity with different thickness distribution as shown in Fig. 2. The gate position found was 26.31 mm from the left side. In addition, the width and land length of the gate minimizing both shear stress and shear rate were 11.8 mm and 2.0 mm, respectively. From the plot of the melt front advancement at the end of the filling shown in Fig. 3, it can be seen that the fan gate designed satisfies the flow balance very well.

Table 1 Parameters in Cross Model

n	0.17447
$\tau^*(P_a)$	8.1002×10^5
$D_1(P_a s)$	1.19×10^{12}
$D_2(K)$	417.0
$D_3(K/P_a)$	0.0
A_1	28.407
$\tilde{A}_2(K)$	51.6

Table 2 Parameters in Tait Equation

Data Unit	Melt	Glass
$a_o(m^3/Kg)$	8.6531×10^{-4}	8.6531×10^{-4}
$a_1(m^3/KgK)$	5.55×10^{-7}	2.27×10^{-7}
$B_o(P_a)$	1.7×10^8	2.61×10^8
$B_1(1/K)$	4.4286×10^{-3}	2.5282×10^{-3}
$T_{go}(K)$	417.15	
$B_2(K/P_a)$	4.46×10^{-7}	

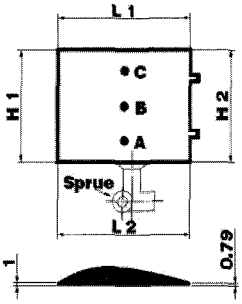

Fig. 2 Configuration of the mold cavity

Table 3 Processing Conditions

Parameters	Processing Conditions
Melt Temperature (^oC)	310
Mold Temperature (^oC)	120
Fill Time (sec)	0.25
Max. Pack Pressure (MP_a)	109.5
Holding Time (sec)	6

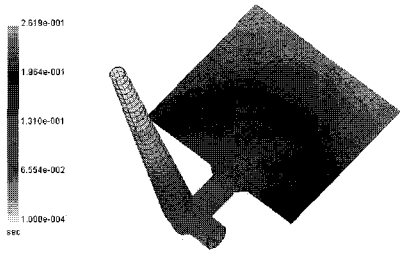

Fig. 3 Melt front advancement

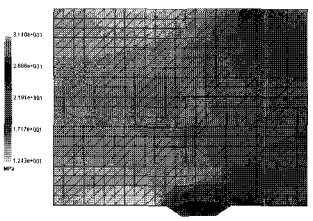

Fig. 4 The distribution of thermal stresses in x-direction before ejection

Fig.4 shows the predicted thermal stresses in the x-direction before ejection. They are under tension, and the maximum stress is 31.4 MP_a around the gate. It is especially shown that the stress in the right area with the thin thickness is larger than that in the left area with relatively large thickness. After ejection from the mold, the thermal stresses are redistributed. The redistribution causes post-molding deformation. As shown in Fig. 5, the stresses that remain after ejection are very small, and a maximum stress of 5.1 MP_a is remained near the gate.

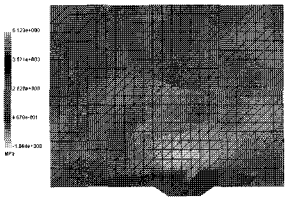

Fig. 5 The distribution of thermal stresses in x-direction after ejection

Fig.6 shows the predicted deformed shape of the molded part induced by the redistribution of the stresses after ejection and temperature drop in the air. The displacements of L1 and L2 were 0.142 mm and 0.141 mm, respectively, while the values of H1 and H2 were 0.110 mm. The cavity size was determined based on the predicted deformation, and a mold with two cavities was built.

To compare the predicted deformation with experimental results, injection molding experiments were carried out by using an injection molding machine (FANUC-30A) with the same processing conditions indicated in Table 3. Before the measurement of dimensions, the molded part was allowed to equilibrate in room temperature for 72 hours. The predicted and measured values are compared in Table 4. The predicted values are in good agreement with experimental results within the error range of 20%. The error might be induced by the neglect of stress relaxation in the calculation of residual stresses and the assumption of isotropic material in deformation analysis.

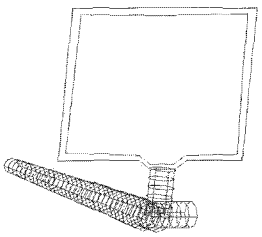

Fig. 6 The deformed shape

Table 4 Comparison between Predicted and Measured Value

Value	δL_1	δL_2	δH_1	δH_2
Predicted Value (mm)	0.142	0.141	0.110	0.110
Measured Value (mm)	0.158	0.117	0.088	0.108

4. Design of Experiments

For one to view the display comfortably under a variety of ambient light conditions from dark to full sunlight, the LGP should provide adequate brightness and uniformity, while minimizing the power consumption. In this study, a DOE technique was used to investigate the influences of processing conditions on the brightness and uniformity. Especially, among the various DOE techniques, the Taguchi method [14] was used to determine the optimal process parameters for injection molding of the LGP. It uses fractional factorial experimental design, called an orthogonal array, to reduce the number of experiments under permissive reliability. The product parameters are determined such that the product's functional characteristic is optimized with minimal sensitivity to noise. Noise in this instance includes all uncontrollable design factors.

To investigate the relationship between brightness and processing

conditions, the L18 orthogonal array was used. Six controllable factors were identified: fill time (A), holding time (B), melt temperature (C), mold temperature (D), ram speed profile (E), and pack pressure (F). Each factor has three levels, their values, as shown in Table 5. The ram speed profiles (E) were set into 4 steps, 5 steps and 10 steps by using the results of flow analysis for satisfying the constant velocity of melt fronts.

The signal to noise ratio (SN) was used as the response of interest. There was a signal response, calculated from twenty observations, at each of the 18 inner array experimental design points. This response (SN) was calculated over the nine points in the outer array as shown in Fig. 7 for each cavity. Since the objective is to make the brightness as large as possible, SN ratio is calculated as:

$$\eta_i = -10\log_{10}\frac{1}{18}\sum_{j=1}^{18}\frac{1}{y_{ij}^2} \tag{36}$$

where η_i is the SN ratio at i-th experiment and y_{ij} is the brightness at position j indicated in Fig. 7. After injection molding based on the L18 orthogonal arrays, the brightness was measured at 9 positions on the upper and lower cavity with a luminance meter (BM-7 from Topcon Corporation). Using Eq. (36), the SN ratios for each of the 18 experimental conditions were calculated as shown in Table 6.

The SN ratios were also analyzed using the analysis of variance (ANOVA) to review the estimates of each effect on brightness and uniformity. The significant factors affecting brightness were fill time (A) and mold temperature (D), whereas the most significant processing factor affecting uniformity was the melt temperature (C). Based on the ANOVA, SN response diagrams were constructed in Figs. 8 and 9, respectively. It can be seen that the brightness and uniformity increase with the increase of melt and mold temperature. A decrease of fill time leads to an increase in brightness, but the fill time has little influence over uniformity. The possible reason is that viscosity, residual stresses, and frozen-in birefringence decrease with increasing melt and mold temperature and decreasing fill time, increasing the brightness of the LGP.

Table 5 Factors and Levels Used in Experiment

Factors	Unit	Levels		
		1	2	3
A. Fill Time	sec	0.5	1	1.5
B. Holding Time	sec	3	4.5	6
C. Melt Temperature	^oC	280	295	310
D. Mold Temperature	^oC	75	90	105
E. Ram Speed Profile	step	4	5	10
F. Pack Pressure	MP_a	80	100	120

Table 6 SN Ratio for Brightness and Uniformity

No	Column No.								SN (dB)	
	e	e	A	B	C	D	E	F	Bright.	Unif.
1	1	1	1	1	1	1	1	1	32.7	34.0
2	1	1	2	2	2	2	2	2	33.5	39.0
3	1	1	3	3	3	3	3	3	36.4	37.4
4	1	2	1	1	2	2	3	3	34.9	38.4
5	1	2	2	2	3	3	1	1	34.1	37.1
6	1	2	3	3	1	1	2	2	29.4	34.1
7	1	3	1	2	1	3	2	3	35.2	37.4
8	1	3	2	3	2	1	3	1	33.3	37.6
9	1	3	3	1	3	2	1	2	32.2	37.9
10	2	1	1	3	3	2	2	1	36.0	38.3
11	2	1	2	1	1	3	3	2	34.5	37.9
12	2	1	3	2	2	1	1	3	31.5	37.2
13	2	2	1	2	3	1	3	2	35.1	38.2
14	2	2	2	3	1	2	1	3	31.7	36.3
15	2	2	3	1	2	3	2	1	33.3	37.6
16	2	3	1	3	2	3	1	2	36.2	37.5
17	2	3	2	1	3	1	2	3	33.1	38.2
18	2	3	3	2	1	2	3	1	31.9	35.7

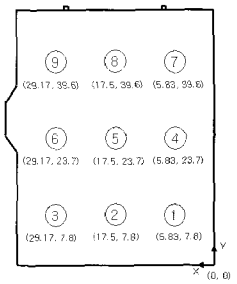

Fig. 7 Measured positions for brightness

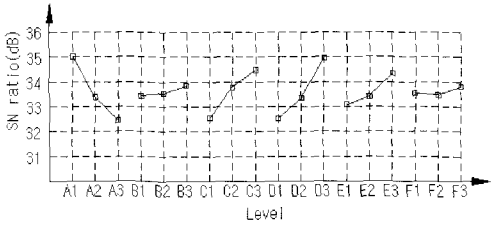

Fig. 8 The SN ratio graph for brightness

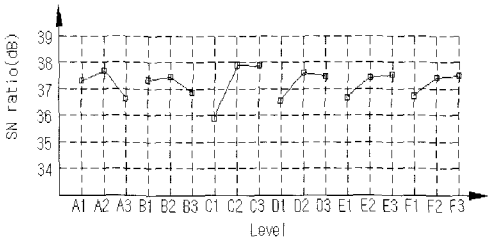

Fig. 9 The SN ratio graph for uniformity

The brightness and uniformity increase with the increase of the step number in setting the ram speed profile. On the other hand, holding time and pack pressure have little influence on the brightness and uniformity. It is believed that the magnitude of brightness depends strongly on the processing parameters in the filling stage.

The optimal selection of all these factors for maximizing brightness and uniformity is $A_1B_3C_3D_3E_3F_3$ or $A_1B_3C_3D_3E_3F_1$. When holding time, ram speed profile, and pack pressure are pooled, the estimated SN ratio is :

$$\eta_{opt} = m + (m_{A1} - m) + (m_{C3} - m) + (m_{D3} - m) = 33.617 + 1.398 + 0.875 + 1.344 = 37.234dB \tag{37}$$

The estimated brightness is $y = 10^{\frac{\eta_{opt}}{20}} = 72.73cd/m^2$ under the selected optimal processing condition. From similar calculation, the estimated uniformity is 81.42 %. The selected optimal processing condition was applied to the verification experiment. The measured brightness and uniformity were 74.21 cd/m^2 and 81.09 %, respectively. The differences between the predicted and experimental values are 2% for brightness and 0.4% for uniformity. The good agreement shows the validity of superposition model used in the Taguchi method. As shown in Table 6, experiment no. 3 has the highest SN ratio of 36.4 dB. The SN ratio is the same with the brightness of 66.1 cd/m^2. Thus, it can be easily seen that the measured brightness under the optimal processing condition selected by the Taguchi method is much larger than the highest value, 66.1 cd/m^2, of the 18 experiments in Table 6. Fig. 10 shows the brightness distribution measured at nine positions after injection molding under the optimal processing condition. There is a large amount of brightness in the middle area of the LGP, but a small amount in the right area, which is relatively thin, and near the gate. This difference in brightness may be due to the formation of frozen-in birefringence in the thin region because the polymer melt has larger stresses due to increased viscosity.

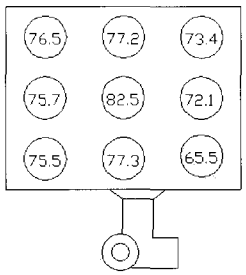

Fig. 10 Brightness distribution

5. Conclusions

Finite element analysis based on the plane stress theory was carried out to predict both the thermal stresses in the post-filling stage and the in-plane deformation after ejection process. The mold cavity was designed based on the predicted deformation, and two-cavity mold was built. The predicted values in deformation were in good agreement with the experimental results within the error range of 20%. To determine the optimal process parameters for injection molding of the LGP, the Taguchi method was used. The brightness and uniformity increased with the increase of melt and mold temperature. Also as the fill time decreased, the brightness increased, while the fill time had little influence over uniformity. Under the optimal processing condition selected by the Taguchi method, the verification experiment showed that the brightness and the uniformity were increased dramatically. The measured brightness and uniformity were 74.21 cd/m^2 and 81.09 %, respectively. There was a large amount of brightness in the middle area of the LGP, but a small amount in the right area, which was relatively thin, and near the gate. The brightness behavior requires more study to establish the relationship between brightness and frozen-in birefringence.

ACKNOWLEDGEMENT

This work was supported by the Korea Research Foundation Grant funded by the Korean Government (MOEHRD) (No. R05-2002-000-00669-0). The author would like also to thank N2A Co. for supporting experiments for this study.

REFERENCES

1. Jacques, M. St., "An analysis of thermal warpage in injection molded flat parts due to unbalanced cooling," Polymer Engineering and Science, Vol. 22, pp. 241, 1982.
2. Tamma, K.K. and Railkar, S.B., "Evaluation of residual thermally induced stresses in the cooling of polymer melt via transfinite element computations," Polymer Engineering and Science, Vol. 29, pp.100-106, 1989.
3. Tamma, K.K., Dowler, B.L. and Railkar, S.B., "Computer Aided Applications to Injection Molding : Transfinite/Finite Element Thermal Stress Response Formulations," Polymer Engineering and Science, Vol. 28, pp. 421-428, 1988.
4. Rezayat, M. and Stafford, R.O., "A Thermoviscoelastic Model for Residual Stress in Injection Molded Thermoplastics," Polymer Engineering and Science, Vol.31, pp. 393-398, 1991.
5. Lee, E.H. and Rogers, T.G., "Solution of Viscoelastic Stress Analysis Problems Using Measured Creep or Relaxation Functions," Journal of Applied Mechanics, Vol.30, pp. 127-133, 1963.
6. Chang, R.Y. and Tsaur, B.D., "Experimental and Theoretical Studies of Shrinkage, Warpage, and Sink Marks of Crystalline Polymer Injection Molded Parts," Polymer Engineering and Science, Vol.35, pp. 1222-1230, 1995.
7. Chang, R.Y. and Chiou, S.Y., "A Unified K-BKZ Model for Residual Stress Analysis of Injection Molded Three-Dimensional Thin Shapes," Polymer Engineering and Science, Vol.35, pp. 1733-1747, 1995.
8. Liu, S.J., "Modeling and Simulation of Thermally Induced Stress and Warpage in Injection Molded Thermoplastics," Polymer Engineering and Science, Vol.36, pp. 807-818, 1996.
9. Santhanam, N., Chiang, H.H., Himasekhar, K., Tuschak, P. and Wang, K.K., "Postmolding and Loas-Induced Deformation Analysis of Plastic Parts in the Injection Molding Process," Advances in Polymer Technology, Vol. 11, 77-89, 1992.
10. Lee, H.S., "In-Plane Deformation Analysis of Plastic Parts in the Injection Molding Process," Journal of Injection Molding Technology, Vol. 3, No. 1, pp. 11-20, 1999.
11. Chiang, H.H., Hieber, N. and Wang, K.K., "A Unified Simulation of the Filling and Postfilling Stages in Injection Molding, part Ⅰ: Formulation and part Ⅱ: Experimental Verification," Polymer Engineering and Science, Vol.31, pp. 116-125, 1991.
12. Hieber, C.A. and Shen, S.F., "A Finite-Element/Finite-Difference Simulation of the Injection Mold Filling Process," J Non-Newt Fluid Mech , Vol. 7, pp.1-32, 1980.
13. C-MOLD Shrinkage & Warpage User's Guide, AC Technology, 1999.
14. Phillip, R., Taguchi Techniques for Quality Engineering; McGraw-Hill Int, 1996.